Developing A Spiral Scanning Method Using Atomic Force Microscopy

Habibullah
SEIT, University of New South Walse
Canberra, ACT-2600, Australia.
Email: h.habib@student.adfa.edu.au

H. R. Pota
SEIT, University of New South Walse
Canberra, ACT-2600, Australia.
Email: h.pota@adfa.edu.au

I. R. Petersen
SEIT, University of New South Walse
Canberra, ACT-2600, Australia.
Email: i.petersen@adfa.edu.au.

***Abstract*—In this paper, we present a spiral scanning method using an atomic force microscope (AFM). A spiral motion is generated by applying slowly varying amplitude sine wave in the X-axis and cosine wave in the Y-axis of the piezoelectric tube (PZT) scanner of the AFM. An LQG controller also designed for damping the resonant mode of the PZT scanner for the lateral positioning of the AFM scanner stage. In this control design, an internal model of the reference sinusoidal signal is introduced with the plant model and an integrator with the system error is introduced. A vibration compensator is also designed and included in the feedback loop with the plant to suppress the vibration of the PZT at the resonant frequency. Experimental results demonstrate the effectiveness of the proposed scheme.**

I. Introduction

Rapid progress of nano-technology is due to the ability to measure, manipulate, and control of matters in nano-scale. Atomic force microscope (AFM) is one of them and it is being used as a tool for characterizing surface topography of material surfaces, biological specimens, etc. with ultrahigh accuracy [1]. The inventions of scanning tunneling microscope (STM), scanning probe microscope such as the AFM, scanning electron microscope (SEM), and transmission electron microscope (TEM) have revolutionized research in various areas such as material science, nano-biotechnology, nano-medicine, nano-pharmaceutics, precision mechanics, optics, microelectronics, etc. [2], [3]. In spite the enormous reputation of the STM, it has some basic demerits, e.g., with the STM one can scan only the electrically conductive samples or those coated with conductive layers. This complicacy was overcome with the invention of the AFM by Binnig [3].

A commercially available AFM scans by applying triangular signal in the X-PZT and a staircase or ramp signal to the Y-PZT. In raster scanning, usually scanning speed is kept limited to 1-10 percent of the first resonant frequency of the PZT scanner [1]. For faster scanning a high frequency triangular signal is needed to be applied. A triangular signal has such characteristics that it contains all odd harmonics of the fundamental frequency. When the triangular signal is input to the PZT, one of the high frequency harmonics excites the resonance and as a result it produces the distorted triangular signal at the free end of the PZT along the X-axis and generates distorted image. In the SPM and other scanner devices such as selective laser sintering machines (SLS) tracking of triangular signal is a major challenge [4].

Researchers are concerned about these challenges and many of them have taken steps to use other feedback control techniques instead of the AFM PI controller to improve the accuracy and speed of the AFM. The signal transformation method is implemented to track the reference triangular signal in AFM [5]. The H^{∞} controller is implemented to improve the scanning speed and image quality, and it achieves a scan rate of 125 Hz [6] . Creep, hysteresis, and vibration effects are minimized by implementing a proportional plus derivative high-gain feedback controller and a feed forward controller [7]. The PZT materials have resonant nature due to their mechanical properties, which is also responsible for distorting the output triangular signal and the scanned images. Therefore the damping of the resonant peak of the PZT is also second major issue in the accurate positioning of the AFM scanner. A survey of the damping controller is given in Ref. [8]. Integral resonant controller is another approach for attenuating the vibration due to the resonant mode of the PZT [9]. In spite of the significant improvements it remains difficulty to track fast triangular signal due to the non-linearities and lower bandwidth of the scanner tube.

To avoid the difficulties associated with the triangular signal, in this paper we propose a spiral scanning pattern instead of raster scanning for the fast AFM imaging. Previously, the spiral scanning approach is introduced in [10]. In this scanning, an externally generated slowly varying amplitudes sine-wave and cosine-wave are applied to the PZT scanner in the X- and Y-axes to force it to move in spiral lines of varying instantaneous radius. This spirals are called Archimedean spiral as shown in Fig. 1. The distance between two consecutive lines is known as pitch p, which has a property that it will be a constant over the sample surface and it makes possible to scan uniformly over the surface without missing surface information. As both the axes are forced by sinusoidal signals with single frequency, the resulting system is in steady-state region and avoid the transient behavior that is occurred in the raster scans because of the probe moving from one line to the next. The proposed scanning method can be included in the faster scanning of the AFM with some software modification.

The reminder of this paper is organized as follows. Description of the AFM and other experimental setup for this work is demonstrated in Section-II. Section-III explains the modeling of the piezoelectric tube actuator. Section-IV discusses the

978-1-4673-5769-2/13/$31.00 ©2013 IEEE

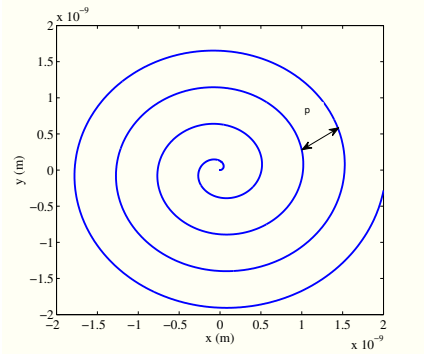

Fig. 1. Spiral lines.

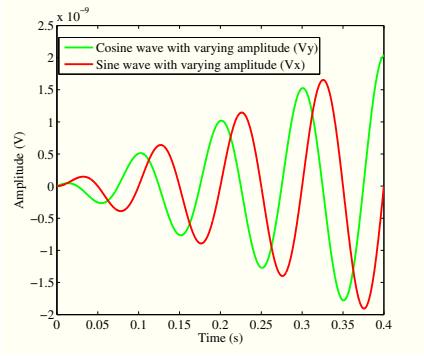

Fig. 2. Input sine wave (V_x) and cosine wave (V_y).

controller design procedure for tracking the reference sinusoids and damping the resonant mode of the PZT. Section-V presents the performance of the controller and finally Section-VI concludes the paper.

II. Generation of Spiral Motion

The area of a sample to be scanned in a spiral trajectory of pitch p at a linear velocity v and if the instantaneous radius R with angular velocity ω (rad/sec) at any time t,

$$\omega = \frac{v}{R} \tag{1}$$

and

$$\frac{dR}{dt} = \frac{p\omega}{2\pi} \tag{2}$$

Integrating eqn.2 we have

$$R = \frac{p\omega t}{2\pi} \tag{3}$$

where R=0 at t=0 and pitch p calculated as:

$$p = \frac{R * 2}{\text{number of spiral curves} - 1} \tag{4}$$

where number of the spiral curves is the number of the crossing points on $y = 0$ or $x = 0$ line. The spirals generated with defined parameter is applied to move the PZT scanner of the AFM in the spiral scanning. To do this eqn. 3 is transformed into Cartesian co-ordinate from polar, as follows:

$$Vx = Rsin\omega t \tag{5}$$

$$Vy = Rcos\omega t \tag{6}$$

where Vx and Vy are the input sine and cosine wave with varying amplitude to the X- and Y-PZT of the AFM scanner, as shown in Fig. 2.

III. Experimental Setup Details

In this work, our experimental setup consists of the NT-MDT Ntegra scanning probe microscope (SPM) that is formed a configuration of the AFM as shown in the Fig. 1. The experiment is carried out in the AFM laboratory at the UNSW@ADFA, Canberra, Australia.

The experimental setup contains some other parts such as signal access module (SAM), control electronics, vibration isolator and a computer to operate the NOVA software. There are some other accessories, these are the signal analyzer (SA), DSP dSPACE board and high voltage amplifier (HVA) with constant gain of 15 to supply power to the X-, Y-, and Z-PZT by using the SAM as an intermediate device. The scanner is a NT-MDT z50313cl PI type: scan by sample and scanning mode was constant force mode. Scan range (X,Y,Z): $100\mu m \times 100\mu m \times 12\mu m$ and resonant frequencies for both the X- and Y-PZTs are 900 Hz, and 5 kHz for Z-PZT, that performs X, Y, and Z positioning in the AFM.

Displacement from X-, Y-, and Z-PZT can be taken from capacitive position sensors which are incorporated with the AFM. The experimental connection is shown in Fig. 3.

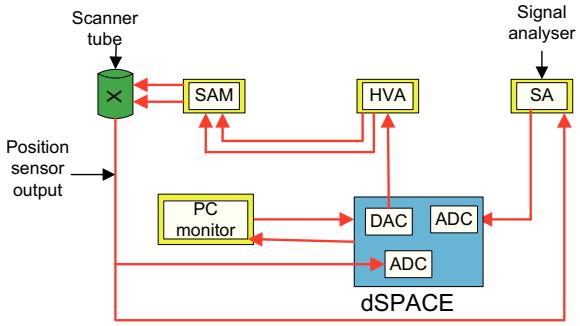

Fig. 3. Block diagram of experimental setup used in the AFM positioning.

Details of the experimental setup can be found in [11].

IV. Modeling of The Piezoelectric Tube Actuator

The PZT actuator is modeled as a single-input and single-output system for designing the proposed control scheme. In the modeling of the PZT a dual channel HP35670A SA is used and from this, a band limited noise signal of 10-1100 Hz is generated which is supplied to the high voltage amplifier (with the gain of 15) as input and amplified voltage is supplied to the SAM of the AFM. There is a direct connection of the SAM with the PZT actuator. The output of the PZT actuator is taken from the position sensor. There are three capacitive sensors to measure the position output of the X-, Y-, and Z-PZT actuators, which are supplied back to the SA output

channel. Thus, a frequency plot is generated in the SA between input and output of the corresponding PZT. As the proposed design approach is based on the lateral positioning, the outputs from X and Y position sensors are considered in this work.

The bode plot generated in the SA is processed in MATLAB and using the system identification tool box and prediction error method (PEM), the system behaviour is characterised [12], [13], and [14]. The best fitted transfer function for the X and Y-PZT are shown in Fig. 4(a) and (b), respectively.

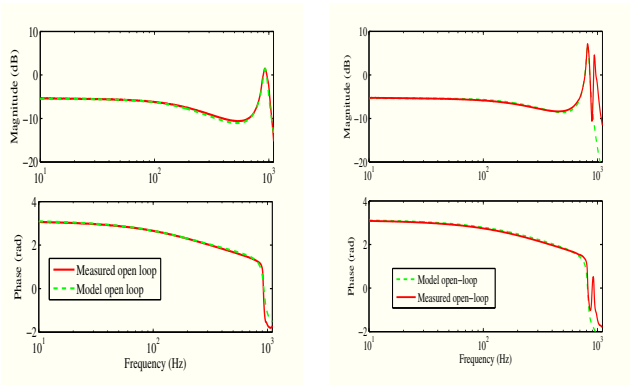

(a) (b)

Fig. 4. Frequency plot of measured and identified system model for (a) input to the X-PZT and output from the X position sensor (b) input to the Y-PZT and output from the Y position sensor.

The following transfer function G_x is found to be a best fitted for the X-PZT as illustrated in Fig. 4(a).

$$G_x = \frac{-16.21\ s^2 + 3.108e004\ s - 9.791e007}{s^3 + 295.3\ s^2 + 8.897e005\ s + 1.843e008} \tag{7}$$

Similarly, the following transfer function G_y is found to be best fitted for the Y-PZT as illustrated in Fig. 4(b).

$$G_y = \frac{-86.46\ s^2 + 4.207e004\ s - 1.116e008}{s^3 + 346.7\ s^2 + 6.851e005\ s + 2.065e008} \tag{8}$$

In Fig. 4 it can be seen that both the PZT plants have a 180° phase at low frequencies and zeros in the right half plane. In the modeling of the PZTs only the first resonant modes are considered.

V. Controller Design

A. Design of LQG Controller for Reference Tracking

The purpose of this section is to present the design of an LQG controller for minimizing the steady-state error and tracking the reference sinusoidal signal. An internal reference model based optimal LQG controller is designed for both the X and Y axes of the PZTs. In this control design, two SISO identified state-space plant models are considered for both the X and Y-PZTs. Let the identified state-space model for the X or Y-PZT be:

$$\dot{x} = ax + bu; \tag{9}$$
$$y = cx + du; \tag{10}$$

where a, b, c, and d are the state-space matrices of the model plant (X-PZT/Y-PZT), as extracted from the eqns. (7) and (8) u is the input, y is the measured output, and $\dot{x}$ is the state vector with dimensions of 3×3.

Let the x be:

$$x = \begin{bmatrix} x_1 \\ x_2 \\ x_3 \end{bmatrix}.$$

One of the objectives of this control design is to control the system error. This error is incorporated in the controller, and to do this, one of the states of the plant is replaced by the error of the system, e.g., x_1 [15]. The system error is defined as the difference between the reference input and plant output as in the following equation:

$$e' = y_r - y; \tag{11}$$

where y_r is the reference input to the plant and assumed to satisfy the differential equation:

$$\dot{\hat{y}_r} = A_r \hat{y_r}; \tag{12}$$
$$A_r = \begin{bmatrix} 0 & -\omega^2 \\ 1 & 0 \end{bmatrix};$$
$$\hat{y_r} = \begin{bmatrix} y_{r_1} \\ y_{r_2} \end{bmatrix};$$

where A_r is the state matrix for the reference signal and ω is the frequency of the input signal. In this design the sinusoidal reference input is modeled and the error dynamic equation is:

$$\dot{e'} = \dot{y_r} - \dot{y}; \tag{13}$$

and to account for the steady-state error an integral action is considered with the error state (e'), i.e.,

$$e'_I = \int e' dt. \tag{14}$$

Now, the error dynamics, i.e., the converted state-space is:

$$\dot{x_e} = Ax_e + Bu_e + Ey_r; \tag{15}$$
$$y_e = Cx_e; \tag{16}$$

where A, B, and C are the state-space matrices of the modified plant, E is the exogenous input matrix, u_e is the input of the modified plant, y_e is the measured output of that plant, and x_e is the state vector with dimensions of a 4×1 matrix, and the state vector of the modified error dynamics model (x_e) is:

$$x_e = \begin{bmatrix} e'_I \\ e' \\ x_2 \\ x_3 \end{bmatrix}.$$

Hence, the entire states (meta-state) of eqns. (12) and (15) satisfies the following differential equation [15],

$$\dot{x_m} = A_m x_m + B_m u_m; \tag{17}$$
$$y_m = C_m x_m; \tag{18}$$

$$A_m = \left[\begin{array}{c|c} A & E \\ \hline 0 & A_r \end{array}\right];$$

$$B_m = \left[\begin{array}{c} B \\ \hline 0 \end{array}\right];$$

$$C_m = \left[\begin{array}{c|c} C & 0 \end{array}\right];$$

where A_m, B_m, and C_m are the state-space matrices of the meta-system, u_m is the input of the meta-system, y_m is the measured output of the plant, and x_m is the meta-state vector. The x_e is the sub-state of the x_m.

Since the exogenous states are generally not controllable, the appropriate performance integral is:

$$J = \int_0^\infty [x_e{}' Q x_e + u_e{}' R u_e] dt; \tag{19}$$

where Q is the state weighting matrix and R is the control weighting, which is scalar. The weighting matrix for the meta system (17) is as follows:

$$Q_m = \left[\begin{array}{c|c} Q & 0 \\ \hline 0 & 0 \end{array}\right];$$

The performance matrix for the meta-system (17) is [15]:

$$\hat{M} = \left[\begin{array}{c|c} \hat{M}_1 & \hat{M}_2 \\ \hline \hat{M}_2{}' & \hat{M}_3 \end{array}\right];$$

where $\hat{M}$ is the performance matrix for the meta-system, $\hat{M}_1$, $\hat{M}_2$, $\hat{M}_2{}'$, and $\hat{M}_3$ are the performance matrices corresponding to the subsystems of the meta-system. Now the gain for the meta-system is:

$$\hat{G_m} = \left[\begin{array}{c|c} R^{-1}B'\hat{M}_1 & R^{-1}B'\hat{M}_2 \end{array}\right];$$

where G_m is composed of the gains $G_e = R^{-1}B'\hat{M}_1$ and $G_r = R^{-1}B'\hat{M}_2$. The G_e is the state feedback gain for the modified plant and G_r is the feed forward gain for the reference input signal which acts against the exogenous effect. The effect of reference signal and external disturbance is known as exogenous effects. An exogenous variable is a factor that is outside of a plant model.

The minimizing matrix $\hat{M}$ that is resulting from minimizing gain $\hat{G_m}$ must satisfy the differential equation for the performance matrices as follows:

$$-\dot{\hat{M}} = \hat{M}A_m + A_m{}'\hat{M} - \hat{M}B_m R^{-1} B_m{}'\hat{M} + Q_m. \tag{20}$$

The solution to this equation will give the gain matrix $\hat{G_m}$. By putting the value of the performance matrix $\hat{M}$ in eqn. 20 and performing matrix multiplication the differential equations for the sub-matrices are obtained as follows:

$$\begin{aligned} -\dot{\hat{M}}_1 &= \hat{M}_1 A + A'\hat{M}_1 - \hat{M}_1 B R^{-1} B'\hat{M}_1 + Q; \\ -\dot{\hat{M}}_2 &= \hat{M}_1 E + \hat{M}_2 A_r + A_c{}'\hat{M}_2; \\ A_c &= A - BR^{-1}B'\hat{M}_1; \end{aligned} \tag{21}$$

where A_c is the closed-loop dynamics matrix of the regulator subsystem and it is seen from $\hat{G_m}$ that the sub-matrix $\hat{M}_3$ of the performance matrix $\hat{M}$ is not needed to find the gain for the meta-system, this is a welcome fact only [15].

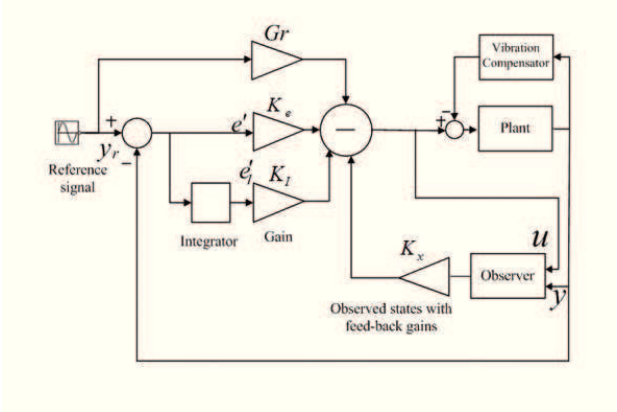

Fig. 5. Block diagram for implementation of the proposed controller.

The steady-state solution for $\hat{M}_2$ can be found and must satisfy:

$$0 = \hat{M}_1 E + \hat{M}_2 A_r + A_c{}'\hat{M}_2; \tag{22}$$

where $\hat{M}_1$ is the solution to the algebraic Ricatti equation of the regulatory sub-system and $\hat{M}_2$ can be found from the above equation. Thus, we have the necessary gains to realize the control law as in [15].

$$u_m = -R^{-1}B'\hat{M}_1 x_e - R^{-1}B'\hat{M}_2 y_r. \tag{23}$$

B. Design of Kalman observer

Kalman observer can be used as a state-observer and noise filter [16]. The displacements of the PZTs are taken from the sub-nanometer resolution position sensors [17]. However, the sensor adds unwanted noise and disturbances to the output displacement taken. To remove this noise we design a Kalman state observer as a noise filter. The sensor measures the output of the PZT plant not the states. As for a regulator system all states of the plant should be known, the Kalman state observer estimates the states from the measured output [15]. The Kalman observer dynamics is follows:

$$\dot{\hat{x}} = (a - Lc)\hat{x} + bu + Ly; \tag{24}$$

$$\hat{y} = \hat{c}\hat{x}; \tag{25}$$

where $\hat{x}$ is the estimated states, $\hat{y}$ is the estimated state output, $\hat{c}$ is the identity matrix of dimension $n \times n$, and L is the observer gain which depends on the Gaussian white noise, process noise covariance, and measurement noise covariance.

C. Design of a vibration compensator

In this section, we discuss the design of a vibration compensator for damping the resonant mode of the PZT. However, the LQG controller has itself the damping capacity, the vibration compensator is introduced to achieve better damping and higher bandwidth. From the experimental frequency responses of the PZTs, we know that the first resonance occurs at 834.5 Hz for the X-PZT and 815.2 Hz for the Y-PZT. The

compensator is designed to damp the first resonant mode of the PZT with a bandwidth close to its first resonant frequency.

The general form of the vibration compensator K_i is given in [18], [19] is:

$$K_i = \sum_{i=1}^{n} -k_{ci} \frac{(s^2 + 2\zeta_i \omega_i \ s)}{s^2 + 2\zeta_i \omega_i \ s + \omega_i{}^2}; \tag{26}$$

where ω_i is the i^{th} is the controller's center frequency which is the frequency at the i^{th} resonant peak of the plant, k_{ci} is the controller gain, and ζ is the damping factor of the corresponding mode. In fact the controller (K_i) is a second-order band-pass filter and has high gain at the resonant frequency of the plant which is means of suppressing the vibration so that the gain suddenly drops away from the resonant frequency. Among the controller parameters, *i.e.*, ω and ζ: ω has a greater effect on damping of the resonant mode than the damping factor (ζ). If we vary ζ by $\pm$ 10 percent, there will be a noticeable effect on damping. But if we vary ω by $\pm$ 5 percent, the attenuation performance will be decreased significantly and once the value of ω is fixed-up the k_{ci} has an important role on damping.

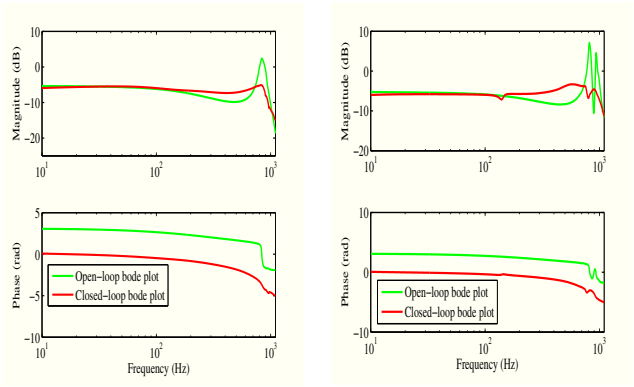

(a) (b)

Fig. 6. Comparison of the frequency responses using an optimal LQG controller with the vibration compensator and open-loop (a) X-PZT and (c) Y-PZT.

VI. Experimental Results

The proposed controller is implemented to the AFM and the frequency domain performance evaluation is presented by the comparison of the measured open-loop and closed-loop frequency response as shown in Figs. 6 for the X and Y-PZT, respectively. The comparison of the measured open-loop and closed-loop frequency response shows the significant damping of the resonant mode of the PZT and higher closed-loop bandwidth close to the first resonant frequency. As a result, the vibration of the PZT is reduced significantly. The frequency plot of the X-PZT has achieved about 9 dB and Y-PZT is about 14 dB damping.

The tracking performance of the proposed controller is shown in Fig. 7 at 10 Hz (tracking of sine and cosine wave) and 30 Hz (tracking of sine and cosine wave). The result shows that the proposed control approach has obtained a good tracking of the reference signal. The spiral tracking of the proposed scheme is shown in Fig. 8. It shows that at 10 Hz phase error is lower than at 30 Hz.

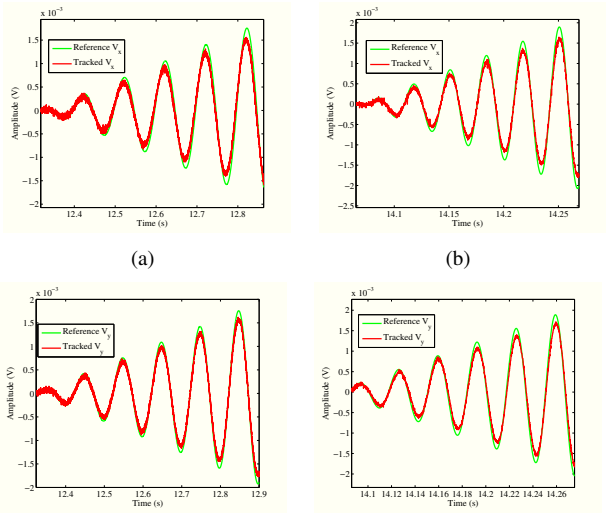

(a) (b)

(c) (d)

Fig. 7. Sinusoidal tracking performance of the proposed controller (a) 10 Hz (sine wave), (b) 30 Hz (sine wave), (c) 10 Hz (cosine wave), and (d) 30 Hz (cosine wave).

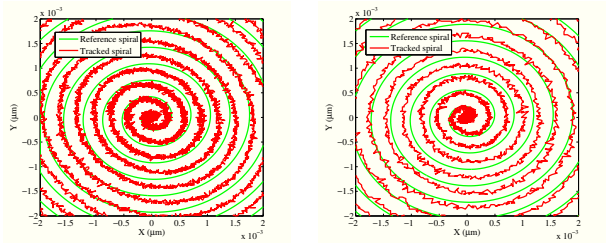

(a) (b)

Fig. 8. Spiral tracking performance of the proposed controller (a) 10 Hz, (b) 30 Hz.

This improved positioning of the PZT scanner is applied to the AFM for the spiral scanning of a TGQ1 standard calibration grating with 20 nm surface height and 3 μm pitch (period). Instantaneous radius of the spiral was maintained at 6 μm and 512 lines, i.e., diameter of the image contains 512 pixel. Constant force AFM imaging mode was setup for spiral scanning and Z-deflection was recorded to construct the spiral image. Here, image scanning results have been observed by implementing the proposed controller in the X- and Y-axes with the help of the real time dSPACE system. The generated spiral images (2D and 3D) are shown in Fig. 9 scanned at 10 Hz, 30 Hz, 50 Hz, and 120 Hz, respectively. The images up to 50 Hz looks undistorted and regular profile of the calibration grating. The effect of non-linear hysteresis and creep, tracking, and vibration of the scanner are not noticeable on the images scanned at 10 Hz, 30 Hz, and 50 Hz. But, 120 Hz image contains effects of the vibrational and dynamics of high speed scanning. At higher speed scanning this effect is severe. The tilting effect of the image can also be observed

at high frequencies. One straight forward thing is that, the 2D planes of the images are not subtracted, that is why there are some uneven illumination in the images as it has done in [10]. This is the reason for imperfections i.e. small misalignments, dust, and additional physical properties.

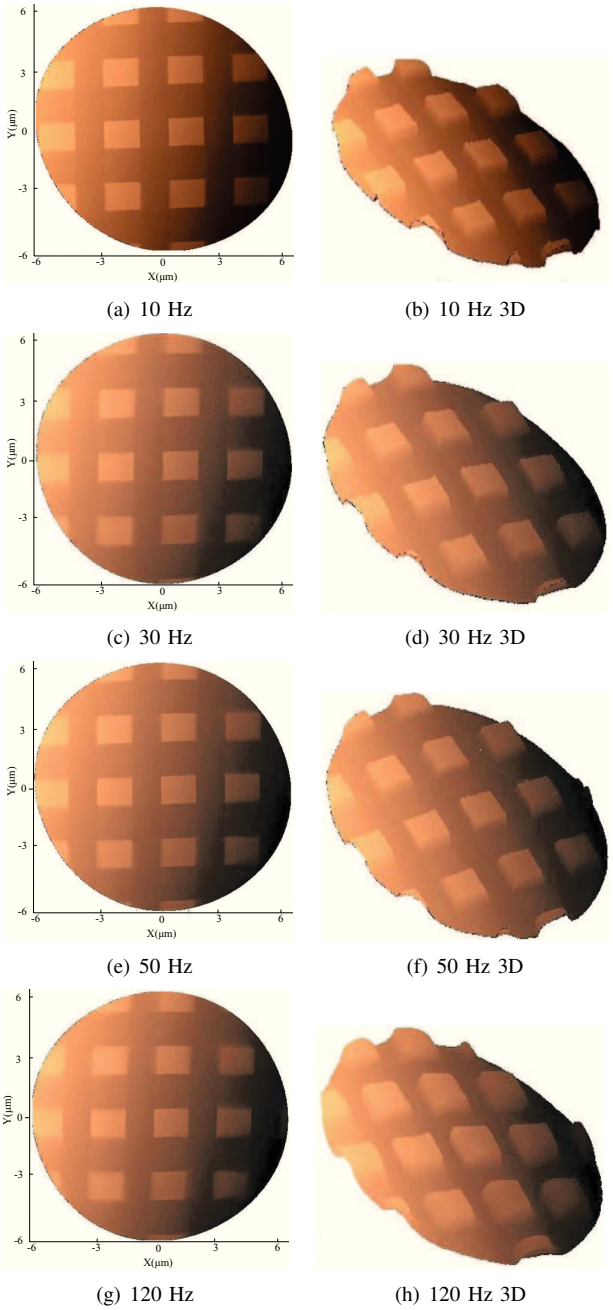

(a) 10 Hz (b) 10 Hz 3D

(c) 30 Hz (d) 30 Hz 3D

(e) 50 Hz (f) 50 Hz 3D

(g) 120 Hz (h) 120 Hz 3D

Fig. 9. Spiral scanned images with the proposed controller (a) 10 Hz 2D, and (b) 10 Hz 3D, (c) 30 Hz 2D, and (d) 30 Hz 3D, (e) 50 Hz 2D, and (f) 50 Hz 3D, (g) 120 Hz 2D, and (h) 120 Hz 3D.

VII. Conclusion

A spiral imaging technique using the AFM is reported in this paper. The proposed controller is implemented to the AFM for the spiral image scanning and experimental results are presented, where it is shown that high speed AFM imaging can be achieved by minimizing hysteresis, creep, vibration and cross-coupling effects. However, at higher frequency scanning, the image is tilted because of phase error due to the cross-coupling among the scanners axes and vibration effect is also noticeable. The phase error could be compensated using phase compensating method.

Acknowledgement

The authors would like to thank very sincerely Mr. Shane Brandon who helps us in our experiments.

References

[1] I. A. Mahmood and S. O. R. Moheimani, "Making a commercial atomic force microscope more accurate and faster using positive position feedback control," *Review of Scientific Instruments*, vol. 80, no. 6, pp. 063 705(1)–063 705(8), 2009.

[2] M. Yves, *Scanning Probe Microscope*, Bellingham, 1995.

[3] G. Binnig, C. F. Quate, and C. Gerber, "Atomic force microscope," *Physical Review Letters*, vol. 56, pp. 930–933, Mar. 1986.

[4] D. Zhiqiang, Z. Zude, A. Wu, and C. Youping, "A linear drive system for the dynamic focus module of SLS machines," *The International Journal of Advanced Manufacturing Technology*, vol. 32, pp. 1211–1216, May. 2007.

[5] A. Bazaei, Y. Yong, S. O. R. Moheimani, and A. Sebastian, "Tracking of triangular references using signal transformation for control of a novel AFM scanner stage," *IEEE Transactions on Control Systems Technology*, vol. 20, no. 2, pp. 453–464, Mar. 2012.

[6] N. Chuang, I. R. Petersen, and H. R. Pota, "Robust H^{∞} control in fast atomic force microscopy," *in Proceedings American Control Conference*, pp. 2258–2265, 2011.

[7] K. Leang and S. Devasia, "Feedback-linearized inverse feedforward for creep, hysteresis, and vibration compensation in AFM piezoactuators," *IEEE Transactions on Control Systems Technology*, vol. 15, no. 5, pp. 927–935, Sep. 2007.

[8] S. Devasia, E. Eleftheriou, and S. O. R. Moheimani, "A survey of control issues in nanopositioning," *IEEE Transactions on Control Systems Technology*, vol. 15, no. 5, pp. 802 –823, Sep. 2007.

[9] B. Bhikkaji and S. O. R. Moheimani, "Integral resonant control of a piezoelectric tube actuator for fast nanoscale positioning," *IEEE/ASME Transactions on Mechatronics*, vol. 13, no. 5, pp. 530–537, Oct. 2008.

[10] I. A. Mahmood, S. O. R. Moheimani, and B. Bhikkaji, "A new scanning method for fast atomic force microscopy," *Nanotechnology, IEEE Transactions on*, vol. 10, no. 2, pp. 203–216, Mar. 2011.

[11] Habibullah, U. R. Obaid, H. R. Pota, and I. R. Petersen, "Internal reference model based optimal LQG controller for atomic force microscope," in *12th International Conference on Automation, Robotics, Control, and Vision, Guangzhou, China*, Dec. 2012, pp. 294–299.

[12] L. Ljung, "Prediction error estimation methods," *Circuits, Systems and Signal Processing*, vol. 21, issue 1, pp. 11–21, Jan./Feb. 2002.

[13] P. Kabaila, "On output-error methods for system identification," *IEEE Transactions on Automatic Control*, vol. 28, no. 1, pp. 12–23, Jan. 1983.

[14] T. McKelvey, A. J. Fleming, and S. O. R. Moheimani, "Subspace-based system identification for an acoustic enclosure," *Transactions of the ASME, Journal of Vibration & Acoustics*, vol. 124 Number 3, pp. 414–419, Jul. 2002.

[15] B. Friedland, *Control system design, An introduction to state space methods*. New York: McGraw-Hill, 1986.

[16] K. Chen, Y. Zhang, B. Lazzerini, and R. Yang, "Stochastic noise tolerance: Enhanced full state observer vs. kalman filter from video tracking perspective," *Journal of Electronics (China)*, vol. 27, no. 4, pp. 557–563, Jul. 2010.

[17] A. E. Holman, P. M. L. O. Scholte, W. C. Heerens, and F. Tuinstra, "Analysis of piezo actuators in translation constructions," *Review of Scientific Instruments*, vol. 66, issue 5, pp. 3208–3215, May 1995.

[18] I. R. Petersen and A. Lanzon, "Feedback control of negative-imaginary systems," *IEEE control system magazine on flexible structure*, vol. 30, no. 5, pp. 54–72, Oct. 2010.

[19] H. R. Pota, S. O. R. Moheimani, and M. Smith, "Resonant controllers for smart structures," *Smart Materials and Structures*, vol. 11, no. 1, pp. 1–8, Feb. 2002.